JOURNAL OF RAMAN SPECTROSCOPY, VOL. 26, 63–76 (1995)

Resonance Raman Spectra of Phthalocyanine Monolayers on Different Supports. A Normal Mode Analysis of Zinc Phthalocyanine by Means of the MNDO Method

Barbara J. Palys,* Dirk M. W. van den Ham, Wim Briels and Dirk Feil
Chemical Physics Laboratory, Twente University of Technology, 7500 AE Enschede, The Netherlands

Resonance Raman spectra of monolayers of transition metal phthalocyanines reveal specific interaction with the support. To elucidate its mechanism, Raman spectra of zinc phthalocyanine monolayers were studied. The analysis was based largely on the results of MNDO calculations. Calculated wavenumbers turned out to be in good agreement with the experimental results. It seems plausible that the α-nitrogen atoms dominate the interaction with the support. Calculation results also show that the usually assumed D_{4h} geometry does not represent the true energy minimum but must be considered as the 'mean' of two mesomeric forms.

INTRODUCTION

Among the various modes of conversion of chemical energy into electricity, there is sustained interest in fuel cells operating at temperatures below 100 °C.[1] A major bottleneck in their development lies in the considerable overpotential that accompanies the electrochemical reduction of molecular oxygen. This overpotential can be reduced by the utilization of catalysts such as platinum. N_4-chelates of first-row transition metal phthalocyanines (MPcs) and of the structurally related naphthalocyanines (MNPcs) may offer a substitute for platinum in the electrochemical oxygen reduction.[1] Most promising in this respect are chelates of iron and cobalt.

From electrochemical experiments we know that the catalytic activity and stability of MPc and MNPc layers depend at least in part on the type of supporting material[2,3] and on the type of electrolyte anions.[4] To optimize these effects, the mechanisms of these interactions have to be established. Raman and infrared (IR) spectroscopy are very well suited to this type of study. Resonance Raman spectra of ZnPc monolayers, adsorbed on gold, glass and glassy carbon, reveal differences that have been attributed to their interactions with the support.[5] It can be envisaged that this interaction occurs via the central metal ion or via the nitrogen atoms. The interaction of MPc films with the electrolyte anions possibly lowers the MPc molecular symmetry and consequently changes significantly the Raman spectrum.[6]

To interpret these differences, the normal mode analysis of MPc is indispensable. To account for possible symmetry changes, the analysis should include all Raman-, resonance Raman- and IR-active modes. Raman spectra of MPc have been already analysed by comparison with related compounds.[7–11] Also, some normal mode calculations have been performed: Aroca *et al.*[12] studied the totally symmetric vibrations of various MPcs. Melendres and Maroni[13] made a normal mode analysis including the MPc planar modes of symmetries A_{1g}, B_{1g} and B_{2g}. Their work is applicable for a description of non-resonant Raman spectra. In their studies of resonance excitation profiles of copper and cobalt phthalocyanines, Bovill *et al.*[10] and Bartholomew *et al.*[11] employed a normal mode treatment of nickel octaethylporphyrin,[14] which also includes A_{2g} modes that are active in resonance spectra. Their assignments overlap to some extent with those of Melendres and Maroni,[13] although there are differences that possibly originate from structural differences between phthalocyanines and porphyrins.[15,16]

The ideal normal mode analysis, adequate to examine MPc–support interactions and possible effects due to redox reactions, should include both Raman-active and non-active vibrations of the phthalocyanine molecule. The quantum molecular orbital (MO) methods permit the calculation of all normal frequencies. In such calculations, the force constant matrix contains second derivatives of the energy with respect to all mass-weighted cartesian coordinates (i.e. all force constants are included in the normal mode calculation). The eigenvalues of this matrix give the normal frequencies. The *ab initio* variants of the MO method give good results for both geometry and force constants calculations only if extensive basis sets are used (see, e.g., Ref. 17). For a molecule as large as MPc, a reasonable *ab initio* calculation requires an unrealistic amount of computer time. Therefore, we have chosen a semi-empirical variant of the MO calculation. The semi-empirical hamiltonian is simplified in comparison with the *ab initio* hamiltonian. The MNDO and AM1 methods use the semi-empirical approximations to the least extent. Both MNDO and AM1 have been reported to give good results for geometry and force constant calculations.[18–21] Unfortunately, with the exception of zinc and chromium, MNDO and AM1 parameters for tran-

* Author to whom correspondence should be addressed.

CCC 0377-0486/95/010063-14

Received 28 February 1994
Accepted 20 September 1994

sition metals are still not available. To overcome this difficulty, we studied zinc phthalocyanine (ZnPc) instead of iron or cobalt phthalocyanine, making use of the observation the peak positions in the Raman and IR spectra of MPcs do not depend strongly on the choice of the transition metal.[8–13] The ZnPc geometry was optimized by both MNDO and AM1 calculations. The normal mode analysis was based on MNDO alone. The average error of MNDO wavenumbers is about 10%, but for a particular molecule this error can be much larger (e.g. 20%).[21] A detailed description of MNDO and AM1 methods can be found elsewhere.[22–24]

In this paper, we compare our calculations and assignments with those of other workers.[7–13] We also discuss the calculated deviation of the ZnPc molecule from the usually assumed square-planar (D_{4h}) structure. Finally, we use our assignments to explain the spectral differences of ZnPc monolayers on gold and on glassy carbon supports. The interaction of electrolyte anions with the ZnPc molecule will be the subject of a separate paper.

EXPERIMENTAL

For the recording of IR and Raman spectra of ZnPc powder, we used the commercially available product as obtained.[25] Monolayers of zinc and iron phthalocyanine on glassy carbon and on gold were prepared by adsorption from solutions in concentrated sulphuric acid.[5]

IR spectra of ZnPc in KBr pellets were obtained with a Fourier transform IR spectrometer (Digilab FTS-60).

Raman spectra were obtained with 514.5 nm radiation from an argon ion laser or with 660 nm line of a dye laser (Spectra-Physics Model 375B), operating with DCM dye. Spectra were recorded using either a scanning double monochromator (Jobin-Yvon HGS) spectrometer (excitation at 514.5 nm) or with a confocal Raman microspectrometer (CRM)[26,27] (excitation at 660 nm). The laser power at the sample varied from 2 mW (CRM) to 80 mW (scanning spectrometer). Peak positions are accurate within 2 cm^{-1} for all Raman spectra.

RESULTS

Experimental

To compare calculated and experimental wavenumbers, Raman and IR spectra (Table 1) of ZnPc microcrystalline powder were recorded. Raman spectra were measured using two excitation wavelengths, 660 nm (Fig. 1) and 514.5 nm (Fig. 2). The 660 nm line is in resonance with the Q absorption band. That at 514.5 nm does not coincide with either the Soret (*ca* 350 nm[28]) or the Q band (*ca* 700 nm[28]).

Trends observed for phthalocyanines[7,8,10–12] show that resonance Raman spectra excited in the Q absorption band contain larger contributions from the non-totally symmetric modes than non-resonantly excited

Table 1. Observed and calculated wavenumbers of infrared-active vibrations

	ν/cm^{-1} Calculated		
Observed	A_{2u}	E_u	Assignment
—	32		ν_{69}
—	108		ν_{70}
—		133	ν_{77}
—	259		ν_{71}
—		262	ν_{78}
—		326	ν_{79}
—	327		ν_{72}
—	435		ν_{73}
500		522	ν_{80}
572		582	ν_{81}
636		648	ν_{82}
728	752		ν_{74}
752		770	ν_{83}
878	846		ν_{75}
888		881	ν_{84}
953		936	ν_{85}
1060	1026		ν_{76}
1088[a]		1108[a]	ν^a
1119		1141	ν_{86}
1164		1161	ν_{87}
1210		1210	ν_{88}
1239		1244	ν_{89}
1283		1283	ν_{90}
1333		1333	ν_{91}
1370		1372	ν_{92}
1484		1496	ν_{93}
—		1512	ν_{94}
1584		1555	ν_{95}
1609		1601	ν_{96}
—		1712	ν_{97}
—		1741	ν_{98}
—		1768	ν_{99}
—		3402	ν_{100}
—		3410	ν_{101}
—		3418	ν_{102}
—		3421	ν_{103}

[a] This wavenumber corresponds to the mode with negative force constant (see text).

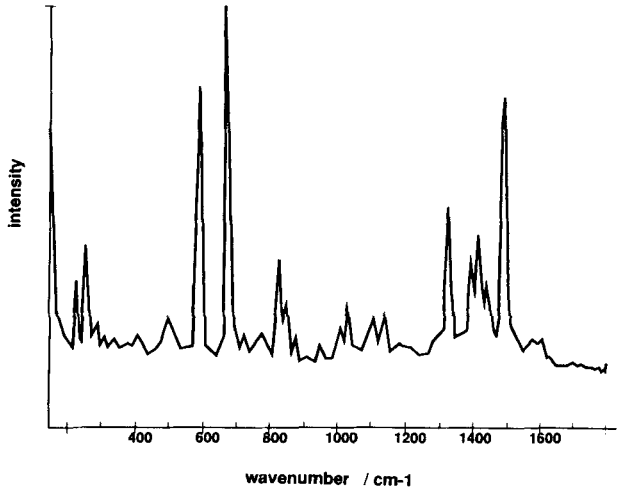

Figure 1. Raman spectrum of ZnPc powder (514.5 nm excitation).

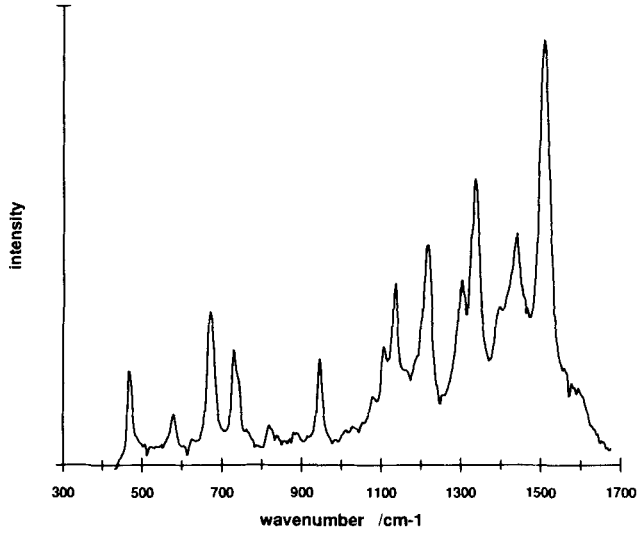

Figure 2. Raman spectrum of ZnPc powder (660 nm excitation). Acquisition time = 30 s.

spectra. Therefore, one would expect the spectra presented in Figs 1 and 2 to be different. In particular, the spectrum excited by 660 nm radiation (Fig. 2) should contain a larger contribution from non-totally symmetric modes. Figs 1 and 2 indeed differ.

To reveal the support–phthalocyanine interaction, resonant-enhanced (660 nm) spectra of ZnPc and FePc monolayers on glassy carbon and on gold were recorded (Figs 3 and 4).

Calculations

The MNDO and AM1 calculations were carried out with the program VAMP4.3[29] on a Convex computer. Both methods allow for the computation of the harmonic wavenumbers by diagonalization of the force constant (Hessian) matrix. Geometry optimization of

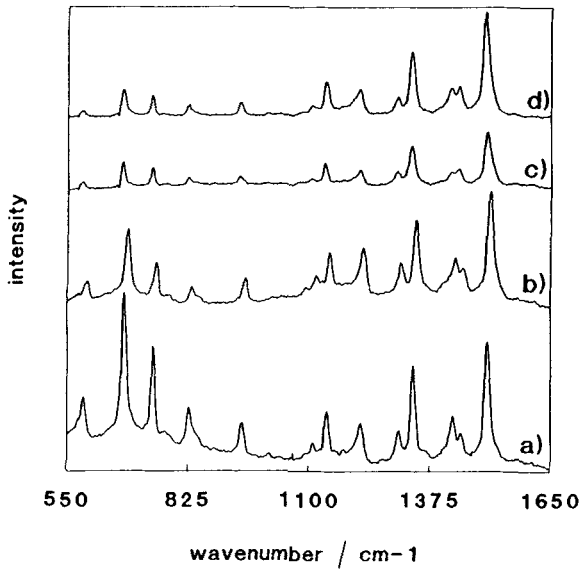

Figure 3. Raman spectra of (a) ZnPc adsorbed on gold; (b) ZnPc adsorbed on gold immersed in 0.1 M $HClO_4$; (c) ZnPc adsorbed on glassy carbon; (d) ZnPc adsorbed on glassy carbon immersed in 0.1 M $HClO_4$ (660 nm. excitation). Acquisition time = 10 s.

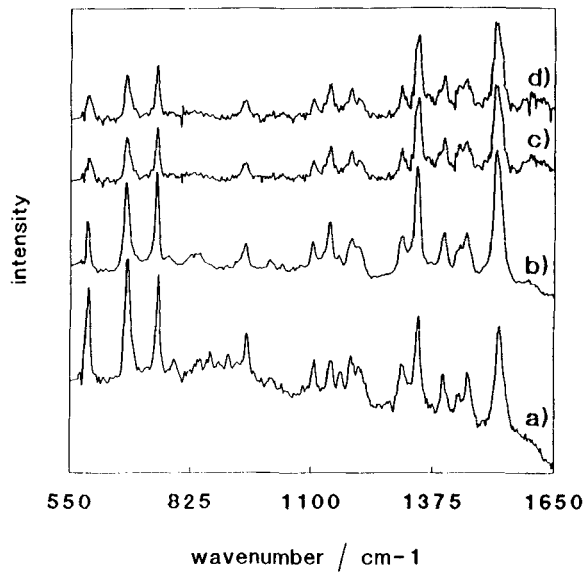

Figure 4. Raman spectra of (a) FePc adsorbed on gold; (b) FePc adsorbed on gold immersed in 0.1 M $HClO_4$; (c) FePc adsorbed on glassy carbon; (d) FePc adsorbed on glassy carbon immersed in 0.1 M $HClO_4$ (660 nm excitation). Acquisition times: (a, b) = 5 s and (c, d) = 30 s.

ZnPc under the constraint of D_{4h} symmetry yielded bond lengths and angles that are close to the experimental x-ray values, albeit that MNDO gave slightly better results than AM1 (Table 2). Because of this and the fact that all other computation results of MNDO, AM1 and unrestricted HF-MNDO do not differ much, we shall restrict the discussion to the MNDO results.

The results depend on whether the D_{4h} constraint is imposed or not. Under this constraint the set of eigenvalues of the Hessian matrix contains two identical negative eigenvalues. The two identical negative eigenvalues correspond to two vibrations of E_u symmetry. The corresponding eigenvectors are presented in Fig. 5 and will be referred to as Q_1 and Q_2. The above nega-

Table 2. Comparison with experiment of the molecular geometries calculated by MNDO and AM1 (atom designations are shown in Fig. 10)

	Bonds	Experimental[35]	MNDO	AM1
Bond distances (Å)	N_α—Zn	1.980	2.018	2.029
	C_α—N_α	1.369	1.392	1.398
	N_β—C_α	1.331	1.342	1.350
	C_β—C_β	1.400	1.422	1.433
	C_γ—C_β	1.393	1.401	1.384
	C_δ—C_γ	1.391	1.410	1.401
	C_δ—C_δ	1.396	1.408	1.396
	H—C_γ	—	1.090	1.100
	H—C_δ	—	1.091	1.101
Bond angles (°)	C_α—N_α—Zn	125.4	125.3	124.8
	C_α—N_α—C_α	109.1	109.3	110.5
	N_β–C_α—N_α	127.8	126.9	128.8
	C_β—C_α—N_α	108.8	109.0	107.9
	C_β—C_β—C_α	106.6	106.3	106.9
	C_γ—C_β—C_β	121.3	120.6	120.8
	C_δ—C_γ—C_β	117.3	118.3	118.0
	C_δ—C_δ—C_γ	121.5	121.1	121.2
	H—C_γ—C_β	—	121.5	121.0
	H—C_δ—C_γ	—	119.4	119.2

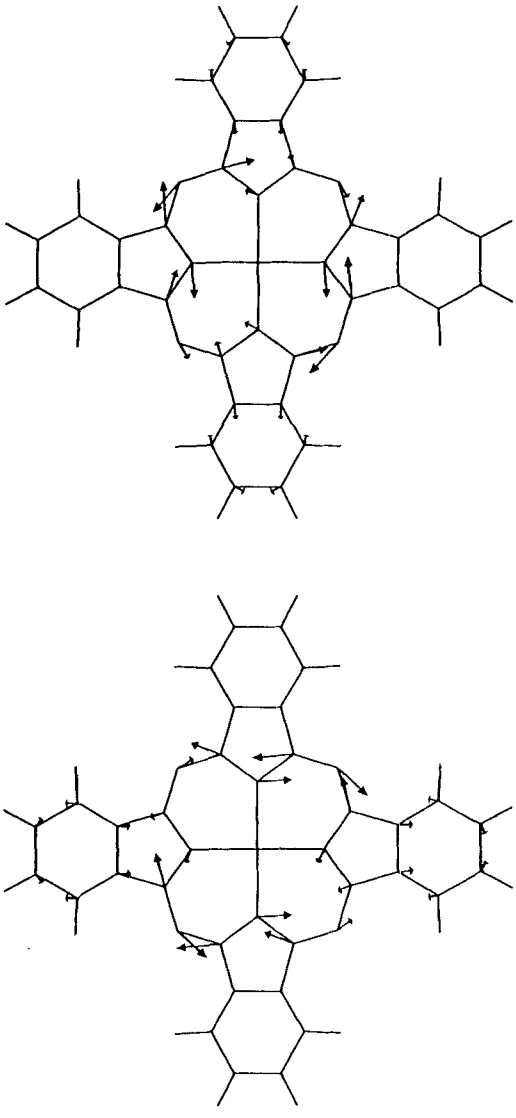

Figure 5. Eigenvectors corresponding to the negative eigenvalues of the force constant matrix.

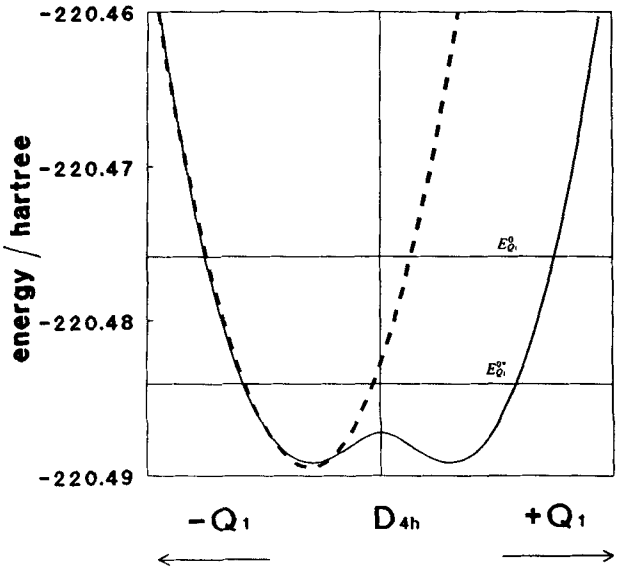

Figure 6. Change of the total molecular energy along the mode with complex frequency. Horizontal axis correspond to the parts of the cartesian displacement vector of this mode (Q_1), which have been added to the optimized D_{4h} geometry. The dashed line would preset the energy of this vibration if we assumed it to be harmonic and the equilibrium geometry corresponded to the minimum of the energy. The zero vibrational energy is $E^0_{Q_1} = \hbar\sqrt{\lambda}$, where λ is the force constant in normal coordinates. $E^{0*}_{Q_1}$ is the zero vibrational energy of the mode when the equilibrium point corresponds to the D_{4h} structure, calculated as in the Appendix.

tive eigenvalues indicate that the square-planar ZnPc molecule will lower its energy by deforming along any linear combination of the vectors Q_1 and Q_2. We therefore examined the dependence of the electronic energy surface on these eigenvectors. The result of addition of only one eigenvector (Q_1) is given in Fig. 6. Addition of linear combinations of Q_1 and Q_2 results in the 'sombrero'-shaped energy surface given in Fig. 7. Inspection of the 'rim' of the 'hat' reveals four of shallow minima of equal depth. The conformations corresponding to the barriers in between those minima are, just like the D_{4h} conformation in the centre of the 'hat,' unstable equilibrium points. The same (stable) minima were found by unconstrained energy minimization, i.e. energy minimization without imposed D_{4h} symmetry. In the conformations corresponding to those minima, the zinc atom is shifted out of the centre of symmetry but remains in the molecular plane (Fig. 8).

The energy surface described above is typical for non-rigid molecules[30] such as ammonia. We shall use this well known example to explain our further calculations on ZnPc.

The stable equilibrium geometry of ammonia has C_{3v} symmetry. Deformation of the molecule along the symmetrical bending mode inverts the molecule to the second stable C_{3v} geometry. The transition state is flat and has D_{3h} symmetry. Diagonalization of the Hessian matrix, corresponding to this transition state, will produce one negative eigenvalue; its eigenvector is the symmetrical bending mode. The energy surface as a function of this mode is similar to that of Fig. 6. The

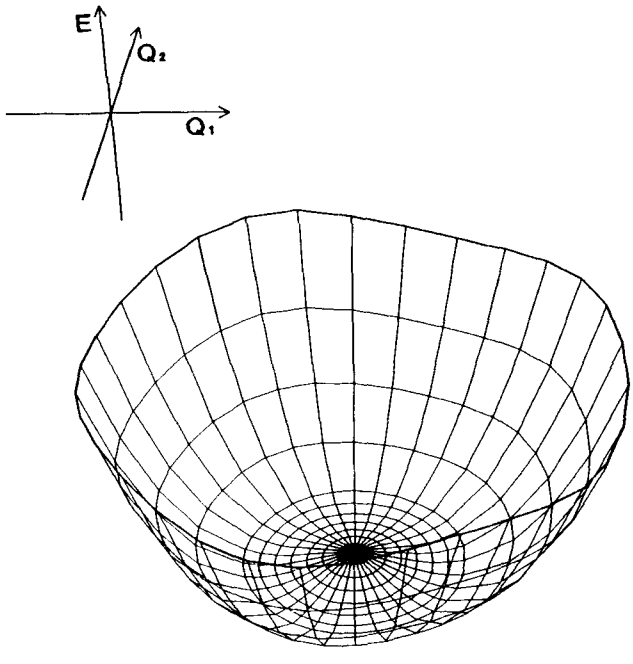

Figure 7. Potential energy surface corresponding to the two degenerate modes with complex frequencies. Q_1, Q_2 as in Fig. 6.

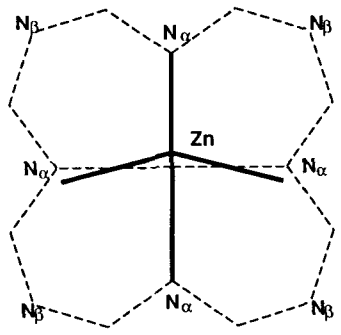

Figure 8. Geometry of ZnPc macrocycle in the minimum of the potential energy surface. The dashed line shows the D_{4h} macrocycle.

second derivatives in both minima are equal and correspond to the symmetric bending modes of the stable conformations. Because of the low barrier between those conformations, the vibrational wavefunctions in different minima overlap. Exact vibrational wavefunctions will be linear combinations of these. The initial degenerate functions give rise to two states with slightly different energies; hence they give rise to the so-called inversion doubling in the vibrational spectrum.

The ZnPc case is nearly analogous to that of ammonia. The main differences are that in ZnPc there are two unstable modes instead of one and that the barriers, including that in the centre, are extremely small (Fig. 7). Owing to the latter, the overlap is large, and the Q_1, and Q_2 wavenumbers will differ strongly from those calculated from the second derivatives in the stable minima. The precise vibrational Hamiltonian (for Q_1 and Q_2 modes) is given in the Appendix.

The nuclear wavefunction of the lowest vibrational state of ZnPc is symmetrically distributed over the four stable minima in the 'rim' and so the molecule can be considered square-planar (D_{4h}) for all practical purposes.

Finally, we want to emphasize that the calculation results discussed above bear absolutely no relationship to the Jahn–Teller effect; the electronic ground state is non-degenerate and the energy difference between ground that first excited states is very large.

Analysis of vibrations

The possible 165 vibrational modes of the (D_{4h}) ZnPc molecule have the following representation: $\Gamma_{vib} = 14A_{1g} + 13A_{2g} + 14B_{1g} + 13E_g + 6A_{1u} + 8A_{2u} + 7B_{1u} + 7B_{2u} + 28E_u$. These modes can be divided into three categories: Raman-active modes, IR-active modes and modes that are neither Raman- nor IR-active (but they become active, as a result of an interaction with the support, if a distortion of the molecular symmetry occurs). The basic Raman selection rules allow A_{1g}, B_{1g}, B_{2g} and E_g modes in the normal Raman scattering. The A_{2g} modes occur in the resonance spectrum as a result of the vibronic coupling between two electronic excited states of phthalocyanine.[31,32] The IR-active modes have A_{2u} or E_u symmetry. The A_{1u}, B_{1u} and B_{2u} modes are normally not observed in Raman or IR spectra. Tables 3, 4 and 5 give the calculated wavenumbers of the Raman-active, IR-active and non-active vibrations, respectively. The ZnPc vibrations are strongly coupled, i.e. delocalized over many internal coordinates. Therefore, the mode description in Tables 3–5 gives groups of atoms which contribute most to the mode concerned.

We restrict the assignment of calculated Raman-active vibrations (A_{1g}, A_{2g}, B_{1g}, B_{2g}, E_g) to the spectral region measured experimentally (200–1700 cm^{-1}). Calculated cartesian displacements for the A_{1g}, A_{2g}, B_{1g} and B_{2g} modes are shown in Fig. 9.

The average error of MNDO frequencies is 10%, but for a particular molecule this error may be much higher (up to 20%). A number of MNDO studies have shown that the wavenumbers are systematically overestimated.[20,21,24] Therefore, we have assumed that the calculated wavenumbers do not depart much from the correct order. We assigned observed bands to the closest calculated (Raman-active) modes. We verified this treatment by comparison with spectra of other metal phthalocyanines;[7–13] differences between relative intensities in spectra excited at 514.5 nm (Fig. 1) and 660 nm radiation (Fig. 2) served as additional information. The non-totally symmetric modes have large relative intensities in the spectrum excited by 660 nm radiation (see above). The proposed assignment is presented in Table 6.

Mode descriptions given by other workers[8–13] do not agree in some respects but a certain 'density of modes' pattern is observed and this agrees with our calculation results. The majority of vibrational assignments indicate that the lowest wavenumber region (below 1000 cm^{-1}) is dominated by macrocycle motions. The macrocycle bending and in-phase movement of pyrrole groups have the lowest wavenumbers (200–300 cm^{-1}).[12,13] Among calculated wavenumbers we find the macrocycle bending mode at 238 cm^{-1} (ν_{30} B_{2g}) and the in-phase translation of isoindole parts (pyrrole groups are included) at 293 cm^{-1} (ν_1 A_{1g}). These vibrations are ascribed to bands observed at 226 and 254 cm^{-1}. The pyrrole translation contributes also to calculated ν_2 (A_{1g}) and ν_{16} (B_{1g}) modes, although benzene motions are significant. Both ν_2 and ν_{16} are assigned to the band observed at 588 cm^{-1}.

The weak feature observed at 283 cm^{-1} possibly corresponds to an out-of-plane deformation of the macrocycle (ν_{46} E_g). The E_g modes are omitted in the existing normal mode assignments.[8–13]

At first sight one might be surprised at the amount of benzene motion in the low-wavenumber modes (ν_1), but this can be understood once one realizes that it is the whole heavy isoindole part that is moving.

The relatively strong band at 468 cm^{-1} is observed exclusively in the spectrum excited by 660 nm radiation (Q-band resonance). There are three calculated wavenumbers which can be assigned to this band: ν_{31} B_{2g} and ν_{57} A_{2g}. Both modes are delocalized over isoindole parts and N_β bridges. Bovill *et al.*[10] and Bartholomew *et al.*[11] assigned this band to an A_{2g} mode. The cartesian displacement vector for this mode closely resembles the ν_{57} in our calculation. Therefore, we assigned ν_{57} to the 468 cm^{-1} band, in spite of the fact that its calculated wavenumber (564 cm^{-1}) depart significantly from the experimental value.

According to our calculation, the two most intense bands (678 and 748 cm^{-1}) in the low-wavenumber region are strongly localized in the macrocycle part (ν_3,

Table 3. Calculated Raman-active vibrations[a]

	Wavenumber	$\tilde{\nu}$/cm^{-1}	Mode description
A_{1g}	ν_1	293	In-phase isoindole
	ν_2	607	In-phase pyrrole, N_β, C–C–C benzene
	ν_3	718	N_β
	ν_4	933	C–N_α–C, C–N_β–C, C–C–C benzene, H–C–C
	ν_5	1157	H–C–C
	ν_6	1196	H–C–C, C–C benzene
	ν_7	1271	H–C–C
	ν_8	1328	N_α, C–C pyrrole + benzene
	ν_9	1506	C–C pyrrole + benzene
	ν_{10}	1565	N_α, C–C pyrrole
	ν_{11}	1718	C–C–C, C–C benzene, H–C–C, N_α
	ν_{12}	1780	C_α, N_β, C–C benzene
	ν_{13}	3410	C–H, C–C–C
	ν_{14}	3421	C–H
B_{1g}	ν_{15}	170	Isoindole out-of-phase
	ν_{16}	571	Pyrrole out-of-phase, C–C–C benzene
	ν_{17}	753	C–N_α–C, C–N_β–C
	ν_{18}	911	C–N_α–C, C–N_β–C, C–C–C benzene, H–C–C
	ν_{19}	1160	H–C–C
	ν_{20}	1197	H–C–C, C–C benzene
	ν_{21}	1275	H–C–C
	ν_{22}	1382	N_α, C–C pyrrole + benzene
	ν_{23}	1494	C–N_α–C, H–C–C
	ν_{24}	1523	C_β–C_β, H–C–C
	ν_{25}	1718	C–C benzene, C–C–C pyrrole
	ν_{26}	1767	N_β, N_α
	ν_{27}	3410	C–H, C–C–C
	ν_{28}	3421	C–H
B_{2g}	ν_{29}	120	Benzene rotation
	ν_{30}	238	Macrocycle bending
	ν_{31}	491	Macrocycle bending, C–C–C, H–C–C
	ν_{32}	703	C–C–C benzene, C–N_β–C
	ν_{33}	939	Macrocycle bending, C–C–C benzene
	ν_{34}	1119	Macrocycle bending, H–C–C, C_β–C_β–C_γ
	ν_{35}	1232	H–C–C
	ν_{36}	1355	H–C–C
	ν_{37}	1443	C–N_α, C–C pyrrole, H–C–C
	ν_{38}	1582	C–C benzene, H–C–C
	ν_{39}	1668	N_β, C_α, N_α
	ν_{40}	1759	C–C benzene, C–C–C pyrrole
	ν_{41}	3402	C–H
	ν_{42}	3418	C–H
E_g	ν_{43}	63	Macrocycle + benzene out-of-plane def.
	ν_{44}	116	Pyrrole out-of-plane
	ν_{45}	245	Macrocycle + benzene out-of-plane def.
	ν_{46}	283	N_α, N_β out-of-plane
	ν_{47}	414	C_β, C_γ–H_γ, N^α out-of-plane
	ν_{48}	467	C–H, C_β, N_β out-of-plane
	ν_{49}	596	C_α–C_β, N_β, C–H out-of-plane
	ν_{50}	738	C–N_α–C out-of-plane bending, N_β out-of-plane
	ν_{51}	810	C–C–C pyrrole out-of-plane bending, H_γ
	ν_{52}	846	H, C benzene out-of-plane
	ν_{53}	962	H, C benzene out-of-plane
	ν_{54}	1026	H, C benzene out-of-plane
	ν_{55}	1065	C–H out-of-plane
A_{2g}	ν_{56}	237	Pyrrole + N_β in-phase rotation, H–C–C
	ν_{57}	564	N_β-C_α in-phase, benzene bending
	ν_{58}	619	Pyrrole bending
	ν_{59}	858	C–C–C benzene, C–N_β-C
	ν_{60}	1175	C–C–C benzene, C–C pyrrole
	ν_{61}	1276	C–C–C benzene + pyrrole, H-C-C,
	ν_{62}	1336	H–C–C, C–N_α
	ν_{63}	1411	C–N_α, C–N_α–C, H–C–C
	ν_{64}	1574	C–C benzene, H–C–C
	ν_{65}	1673	C–N_β, C–N_β–C
	ν_{66}	1747	C–C, C–C–C benzene
	ν_{67}	3402	C–H
	ν_{68}	3418	C–H

Table 4. Infrared-active vibrations[a]

	Wavenumber	$\tilde{\nu}$/cm^{-1}	Mode description
A_{2u}	ν_{69}	32	Zn, N_α, C_δ–H_δ out-of-plane
	ν_{70}	108	Zn, N_β, C_α, out-of-plane
	ν_{71}	259	N_α, C_β out-of-plane
	ν_{72}	327	N_β, N_α out-of-plane
	ν_{73}	435	C_β, C–H, N_β out-of-plane
	ν_{74}	752	C_α, N_α, N_β out-of-plane
	ν_{75}	846	H, C_δ out-of-plane
	ν_{76}	1026	C–H_γ out-of-plane
E_u	ν_{77}	133	Isoindole bending, Zn–N
	ν_{78}	262	N–Zn–N, pyrrole bending, N_β
	ν_{79}	326	N_α–Zn, H–C–C
	ν_{80}	522	Macrocycle bending, C–C–C benzene
	ν_{81}	582	C–C–C benzene, C–N–C
	ν_{82}	648	C–C–C benzene, N_α, C_α
	ν_{83}	770	C–N–C, Zn-N
	ν_{84}	881	C–C–C benzene, C_α, N_β
	ν_{85}	936	C–N–C, Zn-N, C–C–C pyrrole + benzene
	ν_{86}	1141	C–C–C pyrrole + benzene
	ν_{87}	1161	C–C–C benzene, H–C–C
	ν_{88}	1210	C–C benzene, H–C–C
	ν_{89}	1244	H–C–C
	ν_{90}	1283	C–C benzene, H–C–C, C_β
	ν_{91}	1333	H–C_γ–C_β 60%, H–C_δ–$C\gamma$ 18%, C_γ–C_β 6%
	ν_{92}	1372	H–C–C, C–C pyrrole
	ν_{93}	1496	H–C–C, C–C–C pyrrole
	ν_{94}	1512	C–N_α, C–N–C
	ν_{95}	1555	H–C–C, C–C + C–C–C pyrrole
	ν_{96}	1601	C–C pyrrole, C–N–C
	ν_{97}	1712	C–C–C pyrrole + benzene, C–N
	ν_{98}	1741	C–C benzene, pyrrole bending
	ν_{99}	1768	C–C benzene, pyrrole bending, N_β
	ν_{100}	3402	C–H
	ν_{101}	3410	C–H
	ν_{102}	3418	C–H
	ν_{103}	3421	C–H

[a] The frequency of the $Q_1 - Q_2$ mode = 1108 cm^{-1}.

Table 5. Calculated vibrations which are neither Raman-nor infrared-active

	Wavenumber	$\tilde{\nu}$/cm^{-1}	Mode description
A_{1u}	ν_{104}	102	Isoindole out-of-plane def.
	ν_{105}	425	Isoindole out-of-plane def.
	ν_{106}	565	C_α, C–H out-of-plane
	ν_{107}	811	C_β, C_α out-of-plane
	ν_{108}	962	C–H out-of-plane
	ν_{109}	1065	C–H out-of-plane
B_{1u}	ν_{110}	56	C benzene, C–N_β–C, out-of-plane
	ν_{111}	199	C–N_β–C, C benzene, out-of-plane
	ν_{112}	477	C–H, C_β, N_β out-of-plane
	ν_{113}	636	C_α N_β, C_β out-of-plane
	ν_{114}	810	C pyrrole out-of-plane
	ν_{115}	962	C–H, C_β out-of-plane
	ν_{116}	1065	C–H out-of-plane
B_{2u}	ν_{117}	19	C benzene out-of-plane
	ν_{118}	144	Pyrrole + C_6 out-of-plane
	ν_{119}	278	N_α, C_β out-of-plane
	ν_{120}	417	C_β, N_α, C_γ–H_γ out-of-plane
	ν_{121}	717	C_α, N_α out-of-plane
	ν_{122}	846	H, C_δ out-of-plane
	ν_{123}	1026	H, C_γ out-of-plane

ν_{17}). These vibrations contain large contributions from the nitrogen atoms. In the literature the 678 and 748 cm^{-1} bands are ascribed to macrocycle,[8] pyrrole[10–12] or to combined macrocycle–pyrrole motions.[13] Groups of weak bands around 830 and 1020 cm^{-1} correspond to calculated wavenumber of E_g and A_{2g} vibrations.

The series of bands between 1100 and 1200 cm^{-1} contain mainly C–H in-plane bending modes. This spectral range was described similarly by Melendres and Maroni[13] and by Jennings *et al.*[7]

Jennings *et al.*,[7] in a study of Pc solid films, noticed that the spectral range between 1400 and 1450 cm^{-1} depends on the Pc crystallographic form. According to Jennings *et al.*,[7] the spectral region under consideration involves mainly N_α motions. Our calculation supports their assignment.

The description of the strongest band in the phthalocyanine spectrum (1508 cm^{-1}) is not straightforward. This band is often assigned to the totally symmetric C–C pyrrole and C–N_β stretching.[8,10,11] In the analysis of Melendres and Maroni[13] this is C_α–N_α stretching and N–C–N bending modes. Our calculation reveals two vibrations around the wavenumber concerned: ν_9 (A_{1g}) and ν_{24} (B_{1g}) involving pyrrole and benzene (C–C, C–C–C motions). The vibration, which closely resembles this, obtained by Melendres and Maroni[13] was found at 1565 cm^{-1} (ν_{10} A_{1g}). However, the difference in wavenumber is considerable, and we have assigned ν_{10} to the 1508 cm^{-1} band (together with ν_9 and ν_{24}).

The MNDO calculation reveals a number of modes between 1660 and 1780 cm^{-1}. If one assume a 10% calculation error, these modes should be observed around 1600 cm^{-1}. Raman spectra of ZnPc and other metal phthalocyanines reveal only weak bands around 1600 cm^{-1}, which can hardly fit the calculated wavenumbers, but the metal-free phthalocyanine spectrum[8] shows an intense band at 1610 cm^{-1}. Also, spectra of porphyrins show a number of bands between 1550 and 1700 cm^{-1} (e.g. Ref. 14). Furthermore the ν_{25}, ν_{26} and ν_{65} modes of ZnPc closely resemble the ν_{11}, ν_{10} and ν_{19} modes of nickel octaethylporphyrin.[14] For these reasons we consider that wavenumbers calculated between 1660 and 1780 cm^{-1} should be assigned to weak bands around 1600 cm^{-1}.

Existing normal mode treatments of porphyrins and phthalocyanines often emphasize the existence of A_{1g}–B_{1g} and A_{2g}–B_{2g} pairs of closely related vibrations.[10,11,14] In A_{1g} and A_{2g} species adjacent pyrrole rings vibrate in-phase, and in B_{1g} and B_{2g} species out-of-phase. The wavenumber separation is related to the contribution from the bridge atoms.[14] Our calculation results yield similar pairs of vibrations. Among the A_{1g}–B_{1g} species these are ν_1–ν_{15}, ν_2–ν_{16}, ν_4–ν_{18}, ν_5–ν_{19}, ν_6–ν_{20}, ν_7–ν_{21} and ν_8–ν_{22}, and for A_{2g}–B_{2g} species one finds ν_{31}–ν_{57}, ν_{32}–ν_{58}, ν_{35}–ν_{61}, ν_{36}–ν_{62} and ν_{38}–ν_{64} pairs. Comparing these with those calculated by Abe *et al.*[14] for nickel octaethylporphyrin (NiOEP), we notice that both ν_1–ν_{15} and ν_2–ν_{16} include (ν_9, ν_{18}) modes of NiOEP (numbers of vibrations given in parentheses refer to Ref. 33). The pairs ν_1–ν_{15} and ν_2–ν_{16} have different contributions from benzene. One can find also other similarities between ZnPc and NiOEP vibrations: the ν_4–ν_{18} pair includes (ν_7, ν_{15}) of NiOEP, ν_8–ν_{22} includes (ν_5, ν_{14}), and ν_{11}–ν_{25} includes (ν_2, ν_{11}). Among A_{2g}–B_{2g} pairs, ν_{57}–ν_{31} of ZnPc is related to

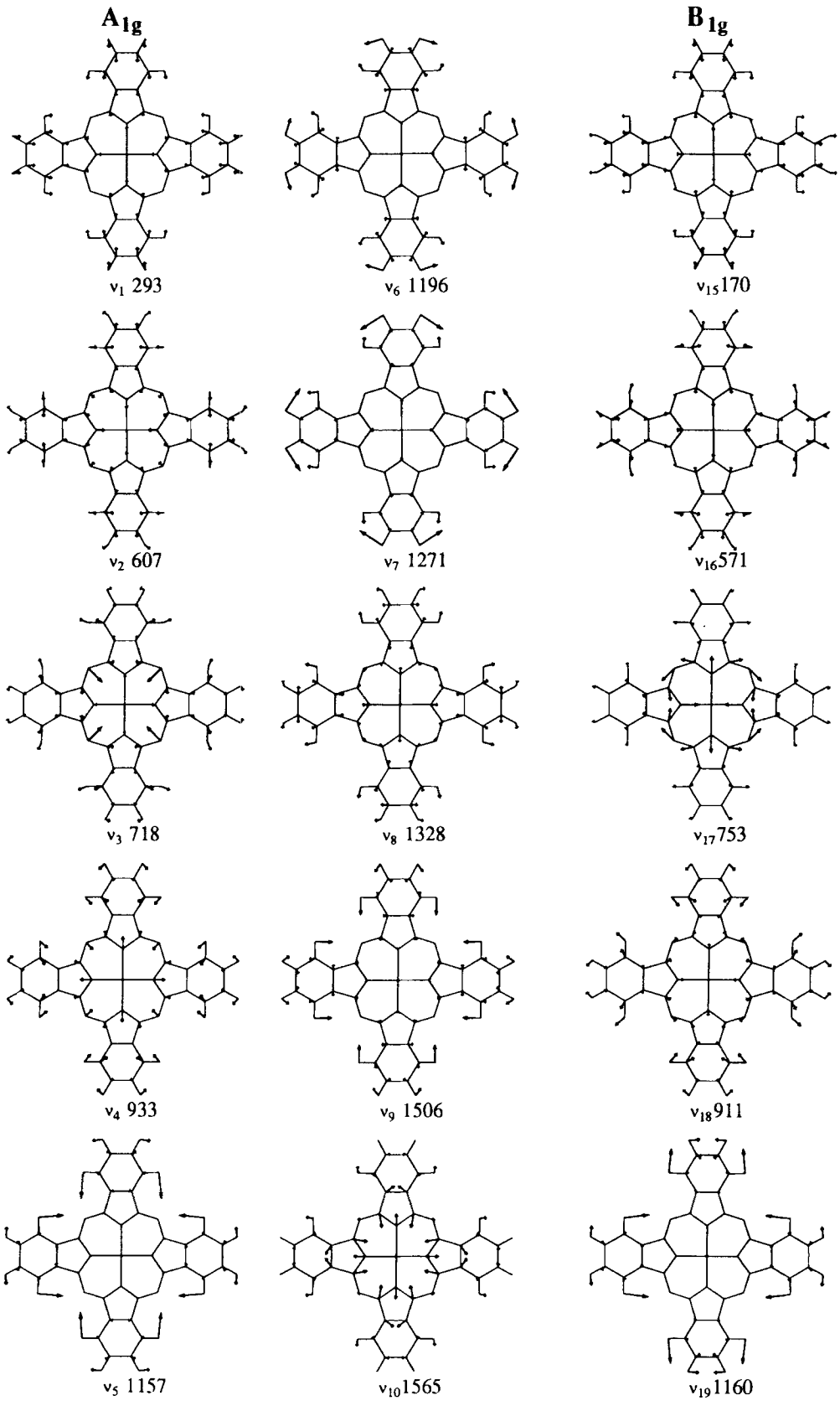

Figure 9. Cartesian displacement vectors for resonance Raman-active, in-plane modes in the 100–1700 cm^{-1} range.

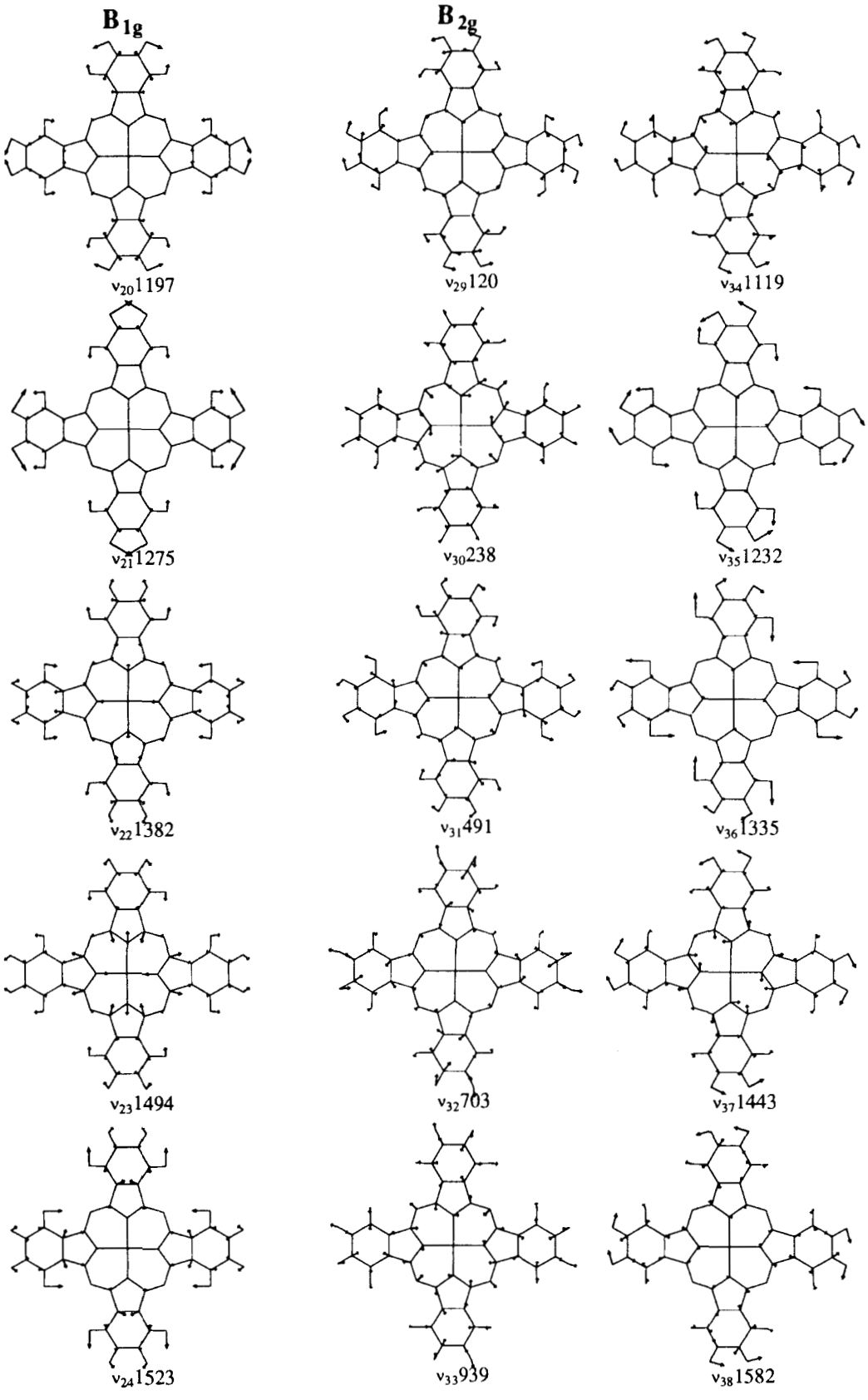

Figure 9. Continued.

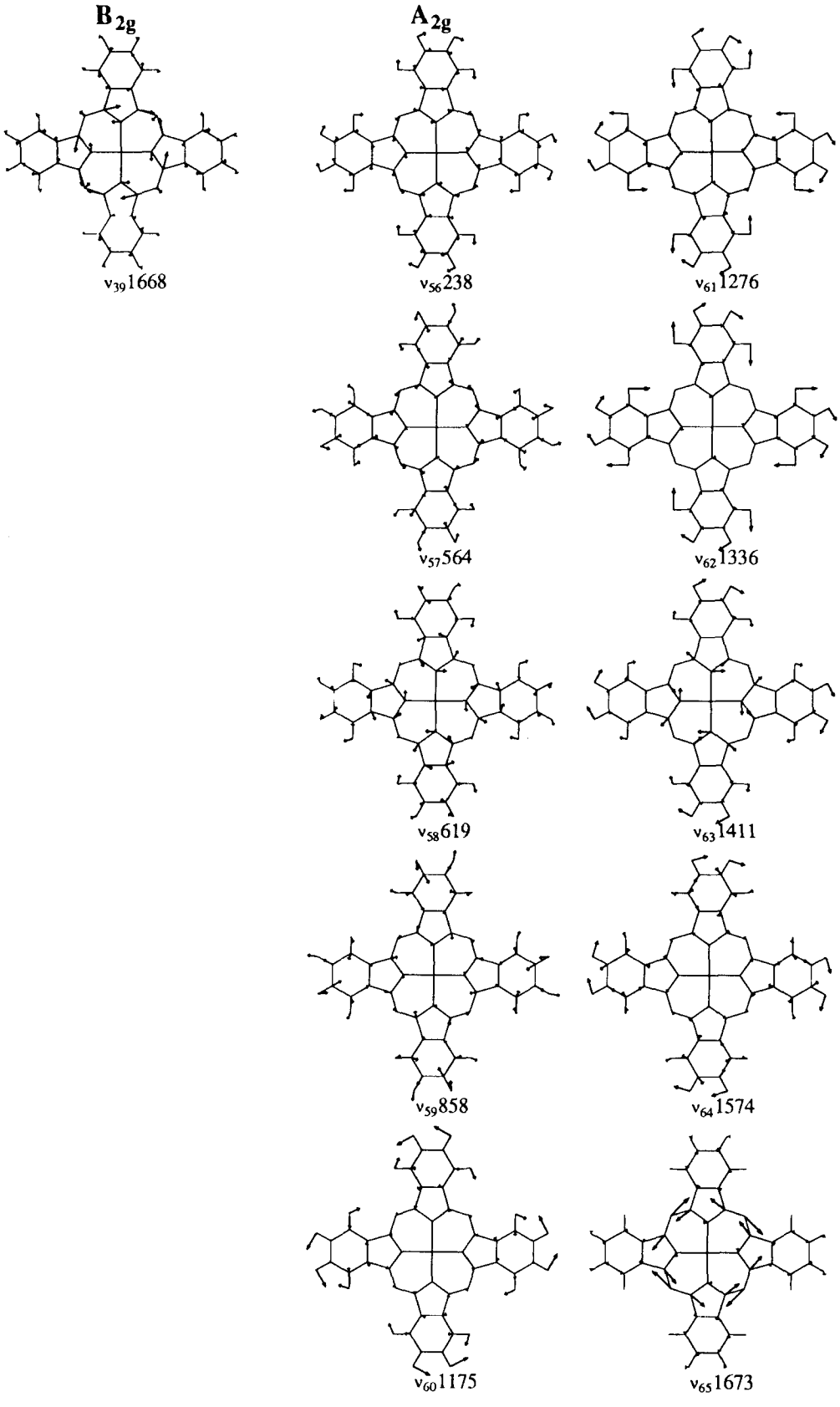

Figure 9. Continued.

Table 6. Assignment of calculated wavenumbers to observed Raman bands

Observed		Calculated wavenumbers (cm^{-1}) and assignment					
Ex. 514.5 nm	Ex. 660 nm	A_{1g}	B_{1g}	B_{2g}	E_g	A_{2g}	
226	—			238			ν_{30}
254	—	293					ν_1
283	—				283		ν_{46}
—	468		491		467	565	$\nu_{31} + \nu_{48} + \nu_{57}$
—	591		571				$\nu_2 + \nu_{16}$
678	678	718		703			$\nu_3 + \nu_{32}$
748	748		753		738		$\nu_{17} + \nu_{50}$
—	826				810		ν^{51}
835	835				846	858	$\nu_{52} + \nu_{59}$
946	946	933	911	939			$\nu_4 + \nu_{18} + \nu_{33}$
1026	1026				962		ν_{53}
1047	1047				1026		ν_{54}
1073	1073				1065		ν_{55}
1107	1107			1119			ν_{34}
1123	—		1160				ν_{19}
1141	1141	1158					ν_5
—	—					1175	ν_{60}
—	—	1196					ν_6
—	—		1197				ν_{20}
—	1217			1232			ν_{35}
1302	1302	1271	1275				$\nu_7 + \nu_{21}$
1335	1335	1328		1335		1336	$\nu_8 + \nu_{36} + \nu_{62}$
1397	1397		1382				ν_{22}
1429	1439			1443		1411	$\nu_{37} + \nu_{63}$
1456	—		1494				ν_{23}
1508	1508	1506	1523				$\nu_9 + \nu_{24} + \nu_{10}$
		1565					
—	—			1582		1574	$\nu_{38} + \nu_{64}$
1600 vw	1600 vw	1718	1718	1688		1673	$\nu_{11} + \nu_{25} + \nu_{39} + \nu_{65}$
		1780	1767	1759		1747	$\nu_{12} + \nu_{26} + \nu_{40} + \nu_{66}$

(ν_{25}, ν_{33}) of NiOEP, ν_{58}–ν_{32} to (ν_{24}, ν_{32}), ν_{63}–ν_{37} to (ν_{21}, ν_{30}) and ν_{64}–ν_{38} to (ν_{20}, ν_{29}). The remaining pairs involve vibrations of benzene, therefore they are not comparable with the porphyrin modes. The correlation between the energy distance of a pair and the N_β contribution is generally confirmed for macrocycle and pyrrole vibrations. Pairs involving benzene motions are nearly degenerate.

In the assignment of calculated infrared-active modes we used data for related MPcs.[12, 34] By comparison of ZnPc spectra with those of related MPcs[12,34] we found three bands of A_{2u} symmetry in the IR spectrum, at 728, 878 and 1060 cm^{-1}. The remaining bands were assigned to the closest calculated E_u mode.

Support interaction

In Fig. 3 we present the Raman spectra of ZnPc (sub)monolayers adsorbed on gold and glassy carbon supports. Comparison of the '*ex situ*' spectra [Fig. 3(a) and (c)] shows differences in relative intensities, but differences in peak wavenumbers fall within the measurement error. The relative band intensities are altered in a similar manner when the ZnPc layers are immersed in an acidic solution [Fig. 3(b) and (d)]. We do not attribute these differences to orientation effects as the roughness of both supports is about the same; moreover, the intensity of the out-of-plane modes (e.g. observed at 827 cm^{-1}) is unaltered. Therefore, the changes in band intensities are possibly caused by an interaction with the support and/or the acidic solution.

Table 7 gives Raman data for ZnPc on glassy carbon, on gold and on both supports in the presence of perchloric acid solution. To facilitate comparison we set the intensity of the band at 1141 cm^{-1} at unity and calculated other intensities in proportion to that band. This particular band was chosen because it contains contributions of benzene and is unlikely to be influenced by an interaction with the support or the acidic solution. The most distinct differences between the spectrum of ZnPc on glassy carbon and on gold are found in the intensities of the 679 and 745 cm^{-1} bands and in the shape of the overlapping bands at 1400–1450 cm^{-1}. According to Table 7, all these vibrations include nitrogen atoms, which suggest that these atoms take part in the interaction with the support. When the ZnPc layer absorbed on gold is immersed in perchloric acid solution, the peaks at 679 and 745 cm^{-1} become weaker [Fig. 3(b)], which makes the spectrum similar to that observed on glassy carbon. When the ZnPc layer is immersed in pure water (pH = 7), no changes are observed. The change in intensity can only be brought about by the absorption of hydrogen ions on nitrogen centres.

The bands at 678 and 745 cm^{-1} change most significantly on contact with acidic solution. The first band corresponds to the mode localised on β-nitrogens (ν_3). The second band involves both N_α and N_β motions (ν_{17}). Hence it is more likely that hydrogen ions are attached to N_β than to N_α centres.

The similarity between the spectrum of the layer adsorbed on glassy carbon and the layer on gold

Table 7. Wavenumbers are relative intensities observed in Raman spectra of ZnPc monolayers adsorbed on glassy carbon and gold supports

	Intensity normalized to 1141 cm^{-1} (ν_5) band of ZnPc adsorbed on[a]				band	Contribution from vibrations involving	
$\tilde{\nu}/cm^{-1}$	Au	$Au/HClO_4$	GC	$GC/HClO_4$	description	N_α	N_β
591	1.0	0.5	0.3	0.4	ν_{16}	+	−
					ν_{57}	+	+
678	3.3	2.0	1.4	1.0	ν_3	−	+
					ν_{32}	−	+
748	2.0	1.1	0.8	0.6	ν_{17}	+	+
					ν_{50}	+	+
826	1.0	0.4	0.4	0.4	ν_{51}	−	−
					ν_{52}	−	−
					ν_{59}	+	+
946	0.9	0.8	0.4	0.5	ν_4	+	+
					ν_{18}	+	+
					ν_{33}	+	+
1108	0.2	0.4	0.2	0.2	ν_{34}	+	+
1141	1.0	1.0	1.0	1.0	ν_5	−	−
1216	0.9	1.6	0.8	1.0	ν_{35}	+	+
1304	0.6	0.9	0.5	0.5	ν_7	+	−
					ν_{21}	−	−
1335	2.2	2.3	1.8	1.9	ν_8	+	+
					ν_{36}	+	−
					ν_{62}	+	−
1427	0.9	1.2	0.6	0.9	ν_{37}	+	−
					ν_{63}	+	−
1450	0.6	0.9	0.8	0.9	ν_{23}	+	+
1508	2.8	3.5	2.7	3.4	ν_9	−	−
					ν_{24}	−	−
					ν_{10}	+	−

[a] Au = gold; $Au/HClO_4$ = gold immersed in 0.1 M $HClO_4$; GC = glassy carbon; $GC/HClO_4$ = glassy carbon immersed in 0.1 M $HClO_4$.

immersed in the acidic solution suggests that in both cases hydrogen ions are attached to N_β centres. This is equivalent to stating that the ZnPc molecule is bound to glassy carbon via acidic groups present on the carbon surface. The spectrum of ZnPc adsorbed on glassy carbon is not affected by contact with perchloric acid solution [Fig. 3(d)], possibly because nitrogen atoms are already attached to acidic surface groups. The effect of hydrogen ions adsorption is less prominent in the case of the overlapping bands between 1400 and 1450 cm^{-1}; they remain characteristic for the type of the support. As these bands include contributions from $Zn–N_\alpha$ stretching and from $C_\alpha–N_\alpha–C_\alpha$ and $N_\alpha–Zn–N_\alpha$ bending modes, we assume that their shape is determined not only by interaction of N atoms with the support or the solution but also by possible bonding to the Zn centre to the support. Since we have already concluded, that nitrogen atoms are involved in ZnPc–glassy carbon bond, we assume that Zn centre takes part in the bonding of the ZnPc molecule to the gold surface.

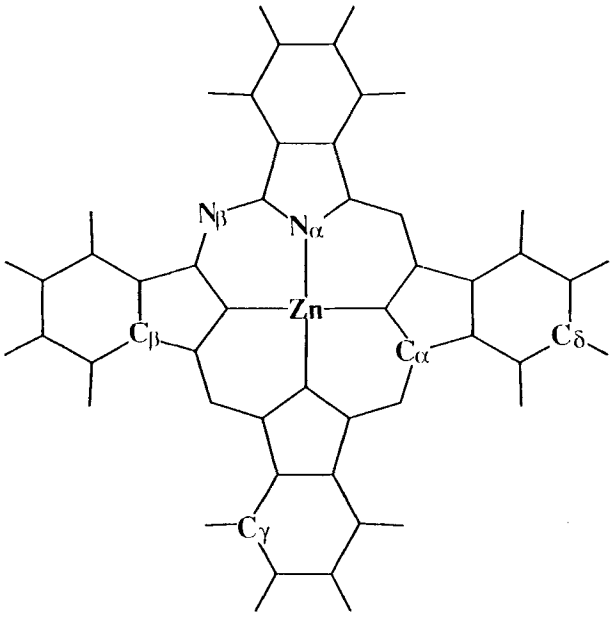

Figure 10. Atom designations for zinc phthalocyanine.

The spectra of iron phthalocyanine monolayers presented in Fig. 4 show similar features to that of zinc phthalocyanine, justifying our choice of ZnPc as the model compound for describing phthalocyanine vibrations.

CONCLUSIONS

Using the MNDO method, accurate results for geometry optimization can be obtained even for molecules as large as ZnPc. The in-plane deformation of the inner ring of the ZnPc molecule lowers the electronic energy. Because the energy gain due to this deformation is smaller than the zero vibrational energy, the ZnPc molecule cannot stay deformed: it oscillates between

equivalent structures and the D_{4h} symmetry is a transition point between them.

Vibrational wavenumbers found by MNDO are close to values obtained experimentally, the differences being of the order of 20–40 cm^{-1} in the spectral region studied. This error is comparable to that of commonly used non-quantum methods. All modes are calculated, also those which are not observed in normal Raman spectra. The mode description obtained in this work agree in general with that published previously.

The calculation results are helpful in explaining the phthalocyanine–support interaction, because by selection of atoms taking part in the molecule–surface bonds, the influence of acid on the Raman spectra of phthalocyanine can also be explained. It has been established that the phthalocyanine molecule is bonded via nitrogen atoms with the glassy carbon surface. However, in case of the gold electrode, the nitrogen atoms do not take part in the binding. Therefore, we assume that the phthalocyanine molecule interacts with the gold surface through the metal ion.

Acknowledgements

The authors are grateful to the Biophysical Technology Group of the University of Twente, particularly to Dr G. J. Puppels and Dr C. Otto, for providing the opportunity to record Raman spectra.

REFERENCES

1. S. Srinivasan, *J. Electrochem. Soc.* **41C**, 136 (1989).
2. A. Billoul, F. Coowar, O. Contamin, G. Scarbeck, M. Savy, D. van den Ham, J. Riga and J. J. Verbist, *J. Electroanal. Chem.* **289**, 189 (1990).
3. F. Coowar, O. Contamin, M. Savy, G. Scarbeck, D. van den Ham, J. Riga and J. J. Verbist, *J. Electroanal. Chem* **282**, 141 (1990).
4. F. Coowar, M. Savy, G. Scarbeck, D. van den Ham, J. Riga and J. J. Verbist, *J. Electroanal. Chem.* **259**, 241 (1990).
5. B. J. Palys, G. J. Puppels, D. van den Ham and D. Feil, *J. Electroanal. Chem.* **326**, 105 (1992).
6. J. L. Kahl, L. R. Faulkner, K. Dwarakanath and H. Tachikawa, *J. Am. Chem. Soc.* **108**, 5434 (1986).
7. C. Jennings, R. Aroca, A.-M. Horr and R. O. Loutfy, *J. Raman Spectrosc.* **15**, 34 (1984).
8. R. Aroca, D. P. DiLella and R. O. Loutfy, *J. Phys. Chem. Solids* **43**, 707 (1982).
9. B. Simic-Glavaski, S. Zecevic and E. B. Yeager, *J. Raman Spectrosc.* **14**, 338 (1983).
10. A. J. Bovill, A. A. McConnell, J. A. Nimmo and W. E. Smith, *J. Phys. Chem.* **90**, 569 (1986).
11. C. R. Bartholomew, A. A. McConnell and W. E. Smith, *J. Raman Spectrosc.* **20**, 595 (1989).
12. R. Aroca, Z. Q. Zeng and J. Mink, *J. Phys. Chem. Solids* **51**, 135 (1990).
13. C. A. Melendres and V. A. Maroni, *J. Raman Spectrosc.* **15**, 319 (1984).
14. M. Abe, T. Kitagawa and Y. Kyogoku, *J. Chem. Phys.* **69**, 4526 (1978).
15. N. H. Sabelli and C. A. Melendres, *J. Phys. Chem.* **86**, 4342 (1982).
16. Li Kao Lee, N. H. Sabelli and P. R. LeBreton, *J. Phys. Chem.* **86**, 3926 (1982).
17. A. Hinchliffe, *Ab Initio Determination of Molecular Properties*. Adam Hilger IOP Publishing, Bristol (1987).
18. M. J. S. Dewar, E. G. Zoebisch, E. F. Healy and J. J. P. Stewart, *J. Am. Chem. Soc.* **107**, 3902 (1985).
19. M. Muller and G. Hohlneicher, *J. Am. Chem. Soc.* **112**, 1273 (1990).
20. C. A. Butler and R. P. Cooney, *J. Raman Spectrosc.* **24**, 199 (1993).
21. M. J. S. Dewar, G. P. Ford, M. L. McKee, H. S. Rzepa, W. Thiel and Y. Yamaguchi, *J. Mol. Struct.* **43**, 135 (1978).
22. M. J. S. Dewar and W. Thiel, *J. Am. Chem. Soc.* **99**, 4899 (1977).
23. M. J. S. Dewar and W. Thiel, *J. Am. Chem. Soc.* **99**, 4907 (1977).
24. J. Sadlej, *Semi-Empirical Methods of Quantum Chemistry*. Ellis Horwood, Chichester (1985).
25. Eastman-Kodak, Rochester, NY 14650; Cat. 134 9968.
26. G. J. Puppels, F. F. M. de Mul, C. Otto, J. Greve, M. Robert-Nicoud, D. J. Arnt-Jovin and T. M. Jovin, *Nature* (London) **347**, 301 (1990).
27. G. J. Puppels, W. Colier, J. H. F. Olminkhof, C. Otto, F. F. M. de Mul and J. Greve, *J. Raman Spectrosc.* **22**, 217 (1991).
28. E. A. Lucia and F. D. Verderame, *J. Chem. Phys.* **4**, 2674 (1968).
29. *VAMP4.3–Vectorized AMPAC*, Convex Computer; AMPAC available from QCPE, program 506.
30. G. Herzberg, *Molecular Spectra and Molecular Structure. Vol. III. Electronic Spectra*, pp. 1–68. Van Norstrand, New York (1966).
31. H. Hamaguchi, *Adv. Infrared Raman Spectrosc.* **12**, 273–310 (1985).
32. D. Dolphin, *The Porphyrins. Vol. III. Physical Chemistry, Part A*. Academic Press, New York (1978).
33. M. Abe, T. Kitagawa and Y. Kyogoku, *J. Chem. Phys.* **69**, 4526 (1978).
34. J. Dowdy, J. J. Hoagland and K. W. Hipps, *J. Phys. Chem.* **95**, 3751 (1991).
35. W. R. Scheidt and W. Dow, *J. Am. Chem. Soc.* **99**, 1101 (1977).

APPENDIX

A brief description is given here of how the vibrational hamiltonian is treated. In the harmonic approximation the hamiltonian reads

$$H = \frac{\hbar}{2}\sum_{j=1}^{F}\frac{\delta^2}{\delta Q_j^2} + \frac{1}{2}\sum_{j=1}^{F}\lambda_j Q_j \qquad \text{(A1)}$$

where the Q_j are mass-weighted normal coordinates and λ_j are related to the wavenumbers $\omega_j = [e_j^{(0)} - e_j^{(1)}]/\hbar$ by $\omega_j = \sqrt{\lambda_j}$; F is the number of degrees of freedom. In the present case it happens that two of the λ_j are negative (we call them λ_1 and λ_2). This simply means that the reference geometry, i.e. that with $Q_j = 0$ for all j, does not represent a stable minimum and that we should look more carefully at the potential energy for higher values of (at least) Q_1 and Q_2. We therefore approximate:

$$H = H_2 - \frac{\hbar}{2}\sum_{j=3}^{F}\frac{\delta^2}{\delta Q_j^2} + \frac{1}{2}\sum_{j=3}^{F}\lambda_j Q_j \qquad \text{(A2)}$$

$$H_2 = -\frac{\hbar}{2}\frac{\delta^2}{\delta Q_1^2} - \frac{\hbar}{2}\frac{\delta^2}{\delta Q_2^2} + V_2(Q_1, Q_2) \qquad \text{(A3)}$$

i.e. we assume that $\omega_3 \ldots \omega_F$ are determined by the second derivatives in the direction $Q_3 \ldots Q_F$, and that ω_1 and ω_2 can be obtained by diagonalization of H_2.

H_2 can be diagonalized on the basis of two-dimensional isotropic harmonic oscillator functions:

$$\chi_{l,m}(r, \varphi) = \frac{1}{\sqrt{\pi}} \sqrt{\frac{1/2(l-m)!}{1/2(l+m)!}} \times e^{-1/2\rho^2} \rho^m L_{1/2(l+m)}(\rho^2) e^{im\varphi} (m \geqslant 0) \times \chi_{l,m}(r, \varphi) = \chi_{l,-m}(r, \varphi)^* (m < 0) \quad \text{(A4)}$$

$$l = 0, 1, 2, 3, \ldots; \qquad m = -1, -1 + 2, \ldots, 1-2, 1$$

where (r, φ) are the polar coordinates in the Q_1, Q_2 plane and $\rho = \sqrt{\gamma} r$. When $V_2(Q_1, Q_2)$ represents an isotropic harmonic oscillator potential with frequency ω the hamiltonian will be diagonal if $\gamma = \omega/\hbar$ is used. When $V_2(Q_1, Q_2)$ is not harmonic but is still isotropic, the function (A4) may still be a good basis. If we restrict the calculation to a finite set of functions, the parameter γ can be used to optimize the basis, i.e., to minimize the energy. Because the hamiltonian will be finally block diagonal in this case, with one block for every m, we can use different parameters γm for different m.

We have calculated the matrix elements by writing

$$H_2 = H_2^{\text{harm}} + H_2^{\text{pert}}$$

$$H_2^{\text{harm}} = -\frac{\hbar}{2} \frac{\delta^2}{\delta {Q_2}^2} - \frac{\hbar}{2} \frac{\delta^2}{\delta {Q_2}^2} + \frac{1}{2} \omega^2 ({Q_1}^2 + {Q_2}^2) \quad \text{(A5)}$$

$$H_2^{\text{pert}} = V_2(Q_1, Q_2) - 1/2\omega^2 ({Q_1}^2 + {Q_2}^2)$$

Using $\omega = \hbar\gamma$, the harmonic part is diagonal; matrix elements of H_2^{pert} have been calculated by means of a numerical integration.